Carbohydrate Polymers 85 (2011) 817–823

Contents lists available at ScienceDirect

Carbohydrate Polymers

journal homepage: www.elsevier.com/locate/carbpol

Cryogenically fabricated three-dimensional chitosan scaffolds with pore size-controlled structures for biomedical applications

Hyeongjin Lee, GeunHyung Kim*

Bio/Nanofluidics Lab, Department of Mechanical Engineering, Chosun University, Gwangju 501-759, Republic of Korea

ARTICLE INFO

Article history:
Received 14 October 2010
Accepted 1 April 2011
Available online 12 April 2011

Keywords:
Chitosan
Biomedical scaffold
Bone tissue regeneration

ABSTRACT

A cryogenic plotting system and manufacturing stage was designed to fabricate three-dimensional (3D) chitosan scaffolds for tissue regeneration applications. The combination of cryogenics and freeze-drying yielded highly porous and structurally stable 3D chitosan scaffolds. The pore size of the chitosan scaffold, which varied from 90 to 400 μm, was reproducibly dependent on processing parameters. Crosslinked chitosan scaffolds exhibited rough surfaces and were stable with regard to shapeability and pore size. During the process, changes in the dimensions of the final scaffold, due to shrinkage and swelling, were within ±10% of the dimensions specified in the initial design. MG-63 cells were cultured on the fabricated scaffolds to evaluate the structures as substrates for tissue regeneration. Cell proliferation on the structured scaffolds was higher than on conventional spongy-type chitosan scaffold. In particular, scaffolds with 200-μm mean pores exhibited the highest rate of cell proliferation.

1. Introduction

To regenerate damaged tissues, cells are attached to and cultured on an appropriate substrate and implanted into or onto the functioning tissue at the injured area. The substrate, commonly referred to as a scaffold, should be biocompatible and made from a biodegradable material that ideally mimics the natural extracellular matrix (ECM) (Yang, Leong, Du, & Chua, 2001). Generally, scaffolds should be highly porous and with an appropriate pore size, large degree of pore interconnectivity, and exhibit a high surface-area-to-volume ratio (Hollister, 2005; Karagenorgiou & Kaplan, 2005). Additionally, the three-dimensional (3D) shape of the scaffold is important for tissue regeneration. According to Lawrence and Madihally (2008), in a two-dimensional scaffold, cell spreading is restricted and cells may only attach to flat surfaces. Any biophysical properties of the substrate that provide spatial–temporal effects in the body are not taken into account. Conversely, it has been shown that the biophysical properties of a substrate can significantly influence both cell adhesion and function in a 3D environment (Huang, Siewe, & Madihally, 2006; Lawrence & Madihally, 2008). 3D substrates can provide both physical and chemical signals to guide cell colonization and to support cell attachment and proliferation, respectively.

Several methods have been used to create scaffolds with ideal spatial architectures (Dalton, Woodfield, & Hutmacher, 2009; Liao et al., 2002; Matthews, Wnek, Simpson, & Bowlin, 2002; Mooney, Baldwin, Suh, Vacanti, & Langer, 1996; Yoon & Park, 2001). These include gas foaming, phase separation, and freeze-drying, which are thermodynamic-based processes, electrospinning, which uses a electrohydrodynamic process, and solid free-form fabrications (SFFs), which include 3D printing, 3D plotting, fused deposition modeling, selective laser sintering, and stereolithography, to construct 3D structures in a layer-by-layer manner. Because layer-by-layer methods can produce scaffolds with complex internal structures that are difficult to prepare with traditional fabrication methods, SFF methods are considered particularly promising (Hollister, 2005; Hutmacher, Sittinger, & Risbud, 2004). These processes are sometimes combined with various conventional fabrication processes, such as electrospinning (Kim, Jang, Park, & Min, 2010; Ma & Choi, 2001; Moroni, Schotel, Hammann, de Wijn, & van Blitterswijk, 2008; Yoon, Ahn, & Kim, 2009) and freeze-drying (Jiankang et al., 2009), to create hierarchical scaffolds with improved cellular behavior. Additionally, recent methods, such as modified photolithography (Jamal, Bassik, Cho, Randall, & Gracias, 2010) and leaching (Choi, Xie, & Xia, 2009), have been proposed for fabricating 3D scaffolds with good cellular responses.

3D biomedical structures have been created with several synthetic biodegradable polymers, including poly(glycolic acid), poly(lactic acid), poly(lactic-co-glycolic acid), and poly(ε-caprolactone). These biopolymers have various advantages, including mechanical flexibility, low antigenicity, easy processability, and low degrees of chronic persistence (Glowacki & Mizuno, 2008). However, disadvantages of these materials for use as biomedical scaffolds include toxicity and the lack of cell recognition signals (Glowacki & Mizuno, 2008). To overcome these disadvan-

* Corresponding author. Fax: +82 62 230 7180.
E-mail address: gkim@chosun.ac.kr (G. Kim).

0144-8617/$ – see front matter © 2011 Elsevier Ltd. All rights reserved.
doi:10.1016/j.carbpol.2011.04.001

tages, natural biopolymers, such as chitosan and collagen, have been widely used as biomedical scaffolds, because they are very similar to macromolecular substances that can be recognized and metabolized in a biological environment (Drury & Mooney, 2003; Glowacki & Mizuno, 2008). In particular, chitosan has been used as a material in tissue regeneration scaffolds, because of its abundance, biocompatibility, biodegradability, antibacterial properties, and wound-healing activity (Kim et al., 2008). Generally, chitosan is derived from the chitin found in crustacean exoskeletons, *e.g.*, crabs, lobsters, and shrimp. Chitosan is a linear polysaccharide, composed of glucosamine and N-acetyl glucosamine units, linked by β(1–4) glycosidic bonds. In biomedical applications, highly porous scaffolds have been formed from chitosan by freeze-drying and by electrospinning micro/nanosized fibers. However, using a direct plotting system, such as one of the aforementioned SFFs, to fabricate a 3D scaffold with chitosan, as opposed to a synthetic polymer, is relatively difficult (Ang et al., 2002). The first reported study detailing the fabrication of 3D chitosan scaffolds using 3D plotting was by Ang et al. Chitosan and chitosan–hydroxyapatite (HA) were dissolved in acetic acid and plotted in a sodium hydroxide–ethanol plotting medium. The resulting chitosan scaffold exhibited an interconnected pore structure, relative to freeze-dried scaffolds. However, the pore interconnectivity structure was incomplete and the porosity at the surface of the scaffold was low.

Recently, we designed the cryogenic system combined with a freeze-drying method and electrospinning process (Ahn et al., 2009; Ahn, Koh, & Kim, 2010; Kim, Ahn, Yoon, Kim, & Chun, 2009). By using this system, we can achieve highly porous 3D collagen scaffolds for skin tissue regeneration. In the current study, we extend this technique to chitosan. In particular, the goal of this work was to adapt the cryogenic direct plotting technique to fabricate chitosan scaffolds, which were mechanically stable, highly porous and had an interconnected pore structure. To assess the feasibility of this material as a scaffold, MG-63 cells were cultured in the scaffold and the cellular response for various mean pore sizes (100, 200, and 400 μm) of the chitosan scaffold was compared with that from a conventionally designed spongy-type chitosan scaffold.

2. Experimental

2.1. Materials

Water soluble chitosan (M_w = 200,000) was obtained from JaKwang Inc. (South Korea). The chitosan solution was prepared in triply distilled water at a fixed concentration of 4.0 wt%. Glutaraldehyde (25 wt%, Sigma, USA) was used to crosslink the chitosan.

2.2. Scaffold fabrication

The cryogenic 3D plotting system (AD-3000C, Ugin-tech, South Korea) included a cryogenic manufacturing stage. The cryogenic refrigeration system consisted of a circulation pump and two compressors that circulated silicone oil to cool the stage. The stage was constantly purged with nitrogen gas to prevent frost formation on the fabricated scaffold due to high ambient humidity. Because the chitosan solution in the nozzle (nozzle diameter = 300 μm) was readily frozen during this process, it was heated to 25 °C. Nozzle speeds varied from 2 to 4 mm/s and the pneumatic pressure was fixed at 225 ± 5 kPa. The design geometry of the chitosan scaffolds was fixed at 20 × 20 × 2 mm^3. The processing temperature of the manufacturing stage was measured using a non-contact infrared thermometer (DT-8860B, CEM). To fabricate chitosan scaffolds, chitosan strands were plotted, layer-by-layer, by extruding the chitosan solution onto a cryogenic plate held at −20 °C. Starting from the bottom layer, each layer adhered to the previous layer and was perpendicular to it, forming a 0°/90° strand structure. The plotted chitosan scaffolds were immediately placed in a freeze-dryer (FD, SFDSM06, Samwon, South Korea) at −76 °C for 2 days. After finishing the freeze-drying process, the scaffolds were cross-linked by immersion in 6 wt% glutaraldehyde for 24 h at room temperature. The scaffolds were then washed copiously in triply distilled water to obtain the final, highly porous chitosan scaffolds. As a control, spongy-type porous chitosan scaffolds were prepared by freeze-drying a chitosan solution (4 wt% in triply distilled water) using the same freeze-drying and cross-linking processes.

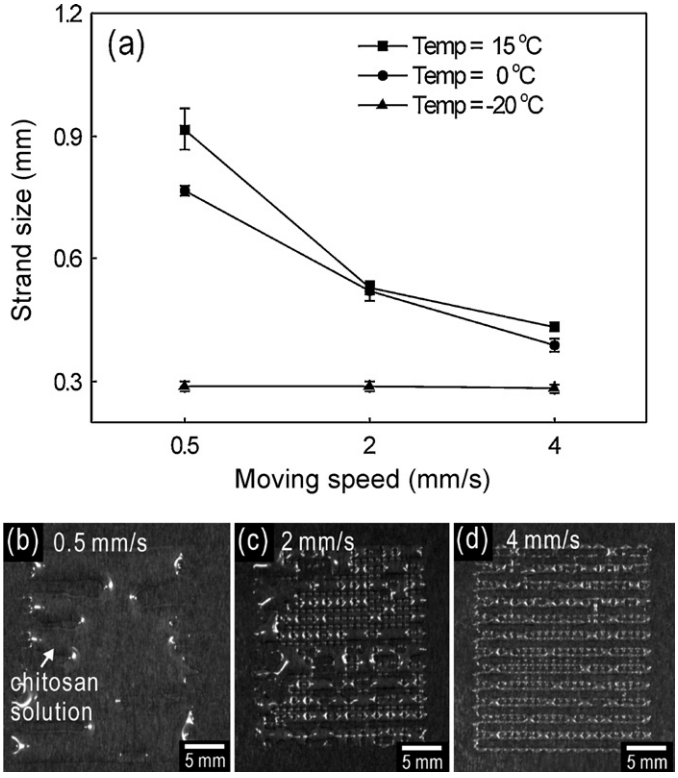

Fig. 1. (a) Single-line chitosan strand diameter at various nozzle speeds and processing temperatures and (b–d) plotted chitosan scaffolds fabricated at 28 °C with various nozzle speeds of 0.5, 2, and 4 mm/s.

2.3. Characterization of 3D chitosan scaffolds

The morphology of the chitosan scaffolds was observed under an optical microscope (BX FM-32; Olympus, Tokyo, Japan), connected to a digital camera, and a scanning electron microscope (SEM, Sirion, FEI, Eindhoven, The Netherlands). The final shape of the structured scaffolds was roughly rectangular and was measured using a digital caliper micrometer (Ultra-cal III, Sylvac). For size measurements, three different parts of the scaffold were measured and averaged. Mechanical properties of the chitosan scaffolds were evaluated by measuring the Young's modulus and maximum strength. The scaffolds were cut into small strips (10 × 18 × 1.8 mm^3). Tensile test was characterized using a universal tensile machine (Top-tech 2000, Chemilab, South Korea). The stress–strain curves of the scaffolds were recorded at a stretching speed of 0.5 mm/s. The scaffold porosity (P) of the cryogenically fabricated chitosan scaffold was calculated as a volume percentage using the equation $P = (1 - M/\rho V) \times 100$, where M is the mass of the scaffold, ρ is the chitosan density (0.5 g/cm^3), and V is the volume of the rectangular scaffold structure. The porosity of the spongy type scaffold was measured by the same procedure of the plotted chitosan scaffold. The scaffold was weighed with a pre-

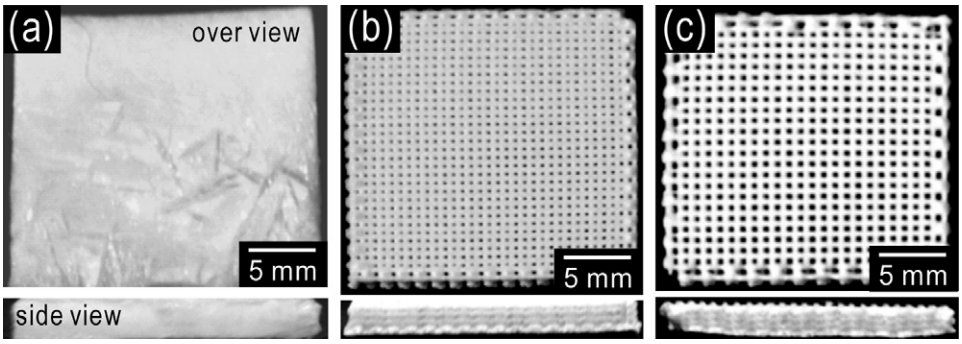

Fig. 2. (a) A spongy-type chitosan scaffold fabricated by freeze-drying and (b and c) 3D structured chitosan scaffolds with 211-μm and 415-μm pores, respectively.

cise balance (AD-4 autobalance; Perkin-Elmer, Waltham, MA). Pore size was assumed to be the distance between chitosan strands and was determined by optical microscopy and SEM. Before the cross-linking process, the pore size of the lyophilized chitosan scaffold was measured in dried state using SEM images and after cross-linking with the glutaraldehyde, the pore size of the chitosan scaffold was measured in phosphate buffered saline (PBS) solution using an optical microscope. All data are expressed as the mean ± standard deviation ($n \geq 5$). Fourier-transform infrared (FTIR) data of the chitosan scaffold were acquired to determine the degree of cross-linking. FTIR data were acquired in attenuated total reflection (ATR) mode using a 6700 FT-IR spectrometer (Nicolet, West Point, PA, USA). Data were acquired for 30 scans between 4000 and 400 cm^{-1} at a resolution of 8 cm^{-1}.

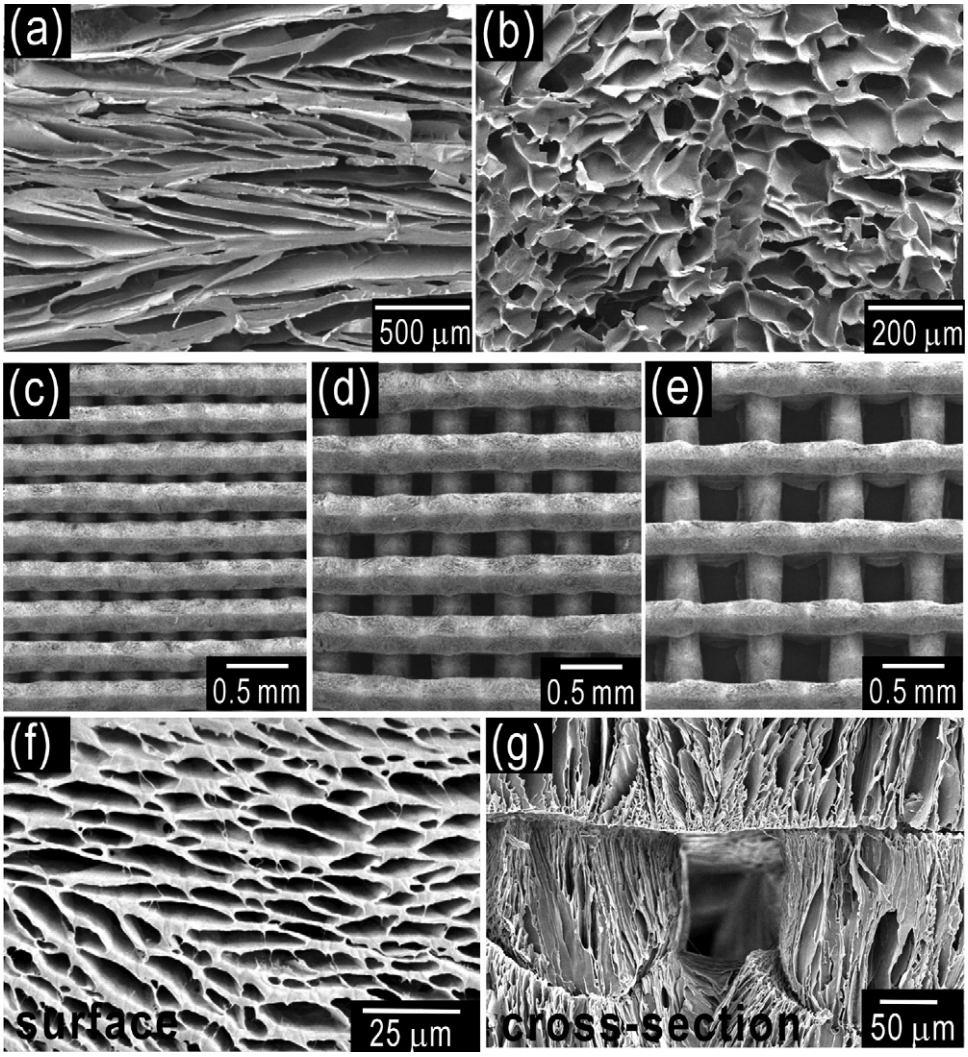

Fig. 3. SEM images of fabricated 3D chitosan scaffolds. (a) Surface and (b) cross-sectional view of a spongy-type chitosan scaffold and structured scaffolds with pore sizes of (c) 92 ± 12 μm, (d) 211 ± 11 μm, and (e) 415 ± 13 μm. (f) An enlargement of the chitosan strand surface and (g) a cross-sectional view of the fabricated scaffold.

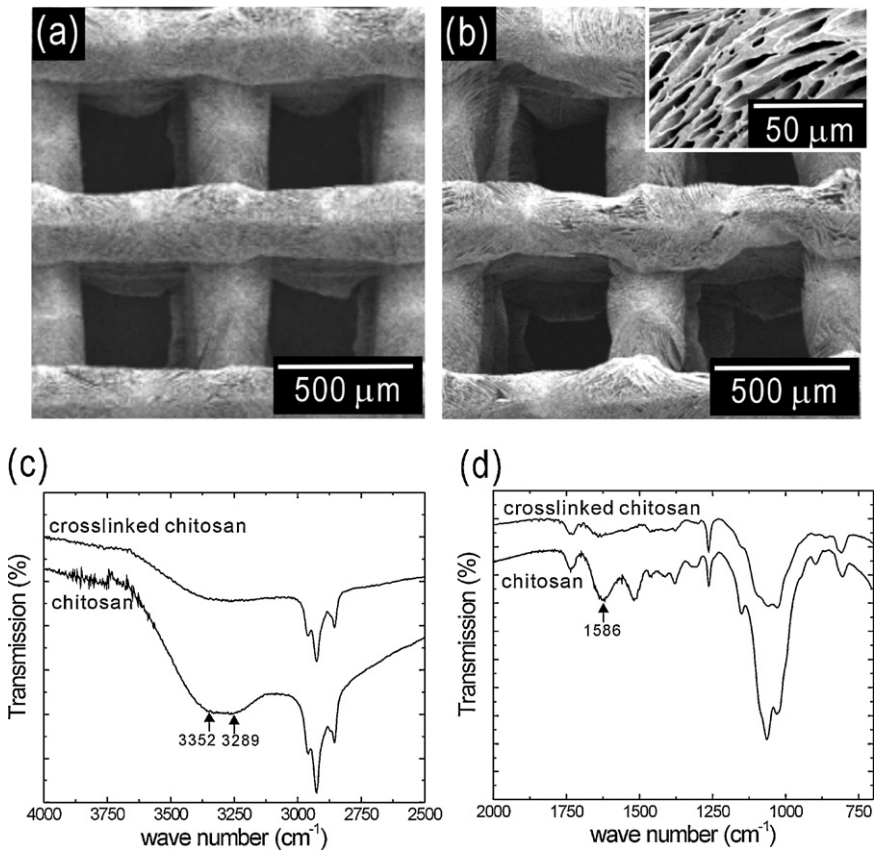

Fig. 4. SEM images show the morphology of the chitosan scaffolds (a) before and (b) after cross-linking with glutaraldehyde; FTIR spectra of the chitosan scaffolds are shown (c) before and (d) after cross-linking.

2.4. Cell culture

Scaffolds for use with cell cultures, $10 \times 10 \times 1.8\,mm^3$, were sterilized with 70% EtOH and UV light, and placed overnight in culture medium. Osteoblasts (MG-63), obtained from ATCC, were used to observe cellular behavior in the chitosan scaffold. MG-63 cells were cultured in Dulbecco's modified Eagle's medium (DMEM, Hyclone, USA), supplemented with 10% fetal bovine serum (FBS, Hyclone, USA) and 1% penicillin/streptomycin (Hyclone, USA). The cells were maintained up to passage 14 and collected by trypsin–EDTA treatment. The cells were then seeded onto the scaffolds at a density of 5×10^4 cells/sample and incubated in an atmosphere of 5% CO_2 at 37 °C. The medium was changed every second day. To assess the morphology of cells on the scaffolds, they were examined by SEM 7 days after seeding. The cell/scaffold constructs were fixed in 2.5% glutaraldehyde and dehydrated through a graded ethanol series. Dried scaffolds were coated with Au and examined under the SEM at 15 kV. Cell growth was determined using an MTT (3-(4,5-dimethylthiazol-2-yl)-2,5-diphenyl tetrazolium bromide) assay (Cell Proliferation Kit I; Boehringer Mannheim, Mannheim, Germany). This assay is based on the cleavage of the yellow tetrazolium salt MTT by mitochondrial dehydrogenases in viable cells to produce purple formazan crystals. Cells on the scaffold were incubated with 0.5 mg/mL MTT for 4 h at 37 °C and the absorbance at 570 nm was measured with a microplate reader (EL800, Biotek Instrument, USA).

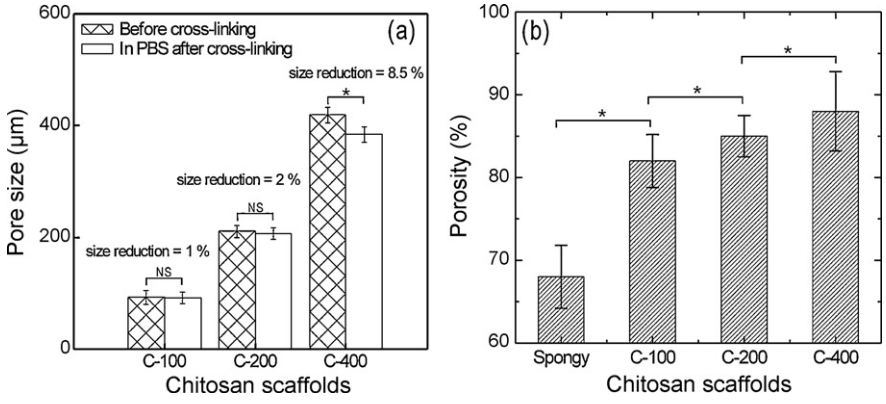

Fig. 5. (a) Pore size before cross-linking and after soaking in PBS solution prior to cell culturing. (b) The porosity of the various cross-linked scaffolds is compared with that of a spongy-type scaffold. NS means non-significant and $^*p < 0.05$.

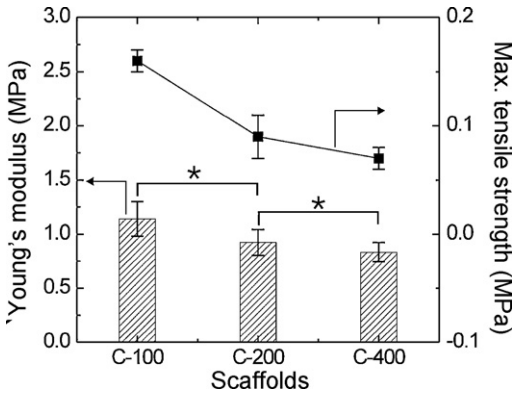

Fig. 6. Young's modulus and maximum tensile strength of the structured chitosan scaffolds is shown as a function of pore size (C-100 = 92 μm, C-200 = 211 μm, C-400 = 415 μm). *$p < 0.05$.

2.5. Statistical analyses

All data presented are expressed as means ± one standard deviation. Statistical analyses consisted of single-factor analyses of variance (ANOVAs). The significance level was set at $p < 0.05$.

3. Results and discussion

The cryogenic plotting system incorporated a dispenser connected to a three-axis moving stage. The temperature of the cryogenic stage and the ambient temperature of the plotting system were fixed at −20 °C and 25 °C, respectively. The pore size stability influences initial cell attachment and proliferation. Thus, the size-stability of the fabricated strands that comprise the 3D scaffold is an essential parameter. As a result, the temperature of the cryogenic stage needs to be optimized under the various processing conditions. The effects of process temperature and nozzle speed on the size of the resulting chitosan strands are shown in Fig. 1(a). Generally, the fabricated strands decreased in diameter as the nozzle speed increased. However, at −20 °C, strand diameter of chitosan solution was independent of nozzle speed and very stable, presumably due to the rapid freezing of the deposition solution. The processing temperature and nozzle speed were thus set to −20 °C and 4 mm/s, respectively. Fig. 1(b) and (d) shows the resulting chitosan plotted at room temperature (28 °C) for various processing speeds (0.5, 2, 4 mm/s). As shown in the figure, although high plotting speed slightly improved the shape-ability of the plotted structure of the chitosan solution, if the appropriate low processing temperature was not applied to the system, the 3D structure of chitosan was not obtained, due to the low viscosity and high hydrophilicity of the deposition solution.

To observe the effect of pore size for bone tissue regeneration, we fabricated three different chitosan scaffolds. Three chitosan scaffolds with pore-sizes of 100, 200, and 400 μm were fabricated using a 300-μm nozzle moving at 4 mm/s. The pore size was controlled by the changing the distance between the microsized strands. Fig. 2(a) shows a spongy-type chitosan scaffold obtained after the freeze-drying process. Fig. 2(b) and (c) shows structured chitosan scaffolds. The fabricated scaffolds had strand diameters ranging from 290 to 310 μm, with pore sizes and overall dimensions differing by less than 10% from the nominally designed pore sizes of 100, 200, and 400 μm: 92 ± 12 μm (C-100), 211 ± 11 μm (C-200), and 415 ± 13 μm (C-400). The total dimensions of the scaffolds were designed to be $20 \times 20 \times 2\ mm^3$; actual measurements were $19 \times 18.7 \times 1.8\ mm^3$.

SEM images showing the surface and cross-sectional morphology of the spongy and structured chitosan scaffolds (C-100, -200, -400) are given in Fig. 3(a)–(g). Fig. 3(a) and (b) shows that evaporation of ice crystals during lyophilization roughened the surface and cross-section of the spongy chitosan. According to several researchers (Dalby et al., 2004; Gadegaard, Martines, Riehle, Seunarine, & Wilkinson, 2006), micro- and nano-sized roughness can influence cell attachment and proliferation on various surfaces. Fig. 3(c)–(e) shows various chitosan scaffolds in which pore size was 100, 200, and 400 μm, respectively. Fig. 3(f) shows a surface of the plotted chitosan scaffold and Fig. 3(g) shows the cross-sectional image of the scaffold (C-100) that had been constructed by layer-by-layer deposition of chitosan microstrands. As shown in the figures, the designed chitosan scaffolds had highly porous structure and the designed pore size was well sustained during the cryogenic process.

The effects of cross-linking on scaffold geometry and surface morphology of micro-sized chitosan strands can be observed in the SEM images before and after cross-linking, shown in Fig. 4(a) and (b), respectively. Both the pore structure and surface roughness were sustained during cross-linking. However, the micro-sized strands shrunk slightly during the dehydration process. These results indicate the formation of stable chitosan scaffolds suitable for cell culturing. Fig. 4(c) and (d) shows FTIR spectra before and after cross-linking. N–H stretching vibrations are observed at approximately 3352 and 3289 cm^{-1} and a peak corresponding to N–H bending is visible at 1586 cm^{-1} in the uncross-linked chitosan. Complete reaction of the amino groups in the cross-linked chitosan scaffold is evident by the absence of any significant amino peaks (Vieira & Beppu, 2006). Thus, the chitosan scaffolds treated with glutaraldehyde were well cross-linked.

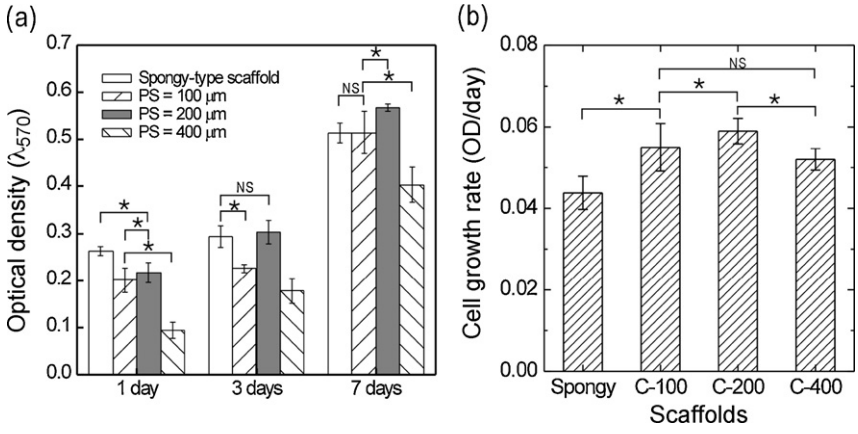

Fig. 7. (a) Cell proliferation results are shown on pore-size controlled chitosan scaffolds and the spongy scaffold; PS = pore size. (b) Cell growth rate vs. various pore sizes (C-100, C-200, C-400). NS means non-significant and *$p < 0.05$.

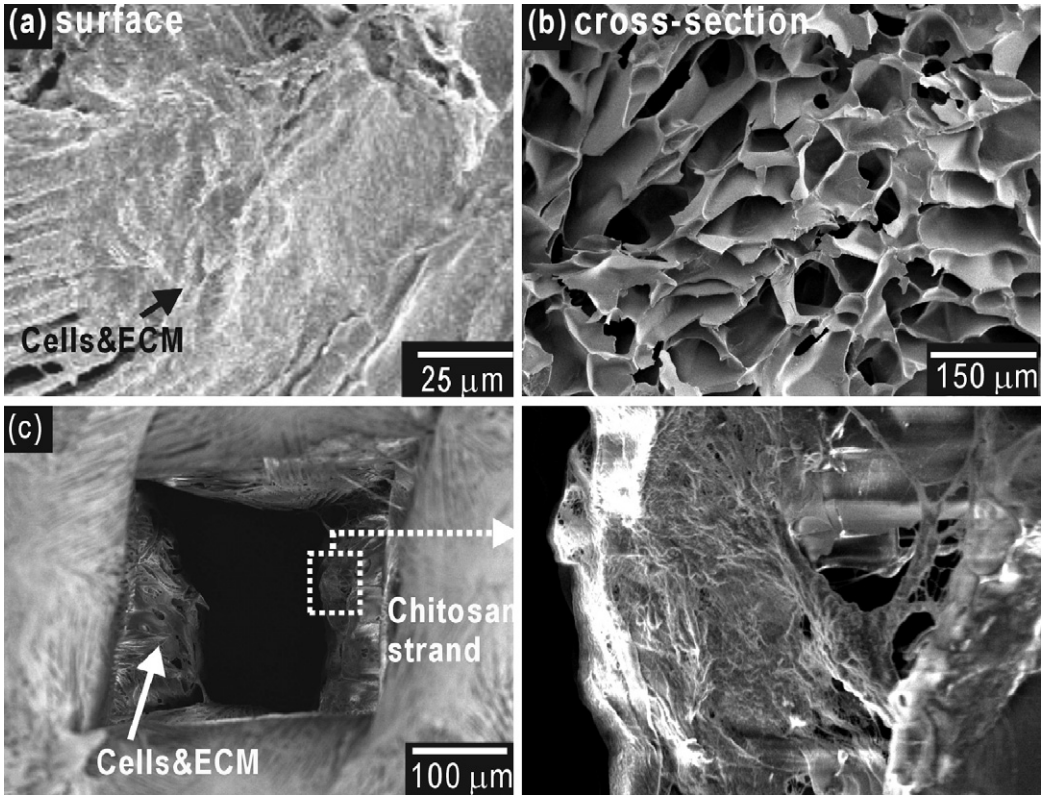

Fig. 8. (a) Surface and (b) cross-sectional SEM images of the spongy type scaffold are shown after seven days of cell culturing; (c) SEM images of the pore-size controlled chitosan scaffold (C-200) seven days after seeding with MG63 cells.

Although controversial, several researchers have suggested optimal pore structures for the regeneration of various tissues. Pore sizes of 100–400 μm and 200–350 μm, have been suggested for tissue regeneration and osteoconduction, respectively, while for fibroblasts and chondrocytes, growth is optimal with pore sizes of 5–15 μm and 70–120 μm, respectively (Oh, Park, Kim, & Lee, 2007). Many researchers agree that different cell lineages exhibit a preference for a particular pore size range. Thus, an optimal scaffold requires a uniformly distributed appropriate pore structure, according to the cells with which it will be used (Choi et al., 2009).

Fig. 5(a) shows the effect of cross-linking on the final pore size of fabricated scaffolds that had been soaked in PBS for 7 days. Fig. 5(a) shows that, although the scaffold was cross-linked, the strands of chitosan swelled slightly, eventually reducing pore size. For all scaffolds (C-100, -200, -400), this reduction was less than 10%, suggesting that changes in scaffold geometry will be sufficiently small to sustain cell cultures.

Fig. 5(b) shows the porosity of spongy chitosan and structured chitosan scaffolds (C-100, -200, -400). As expected, based on the SEM images in Fig. 3, the porosity of structured chitosan scaffolds was enhanced by the artificially designed pore sizes between strands. According to Hutmacher (2000), the porosity of a scaffold must be higher than 85% to support tissue regeneration. In this respect, the structured scaffolds C-200 and C-400 were sufficient, with porosities greater than 85% and up to 90%, respectively. The C-100 scaffold exhibited a porosity of 81% and the spongy chitosan scaffold 68%. These results indicate that the fabrication process described herein is capable of producing chitosan scaffolds with controlled porosity, while maintaining the same chitosan concentration.

Mechanical properties are an important consideration in designing 3D scaffolds, because the injected scaffold in a damaged area can be subject to various stresses. If the scaffold cannot maintain its shape, the emerging hard or soft tissue may be excessively deformed (Drury & Mooney, 2003; Hollister, 2005). According to Williams and Lewis (1982), trabecular bone has a modulus from 38 to 130 MPa. Because bone is an anisotropic material, its modulus depends on the direction of the applied force. The mechanical properties of a structured scaffold depend on the inherent structure and bulk mechanical properties of the materials. The mechanical properties of structured scaffolds are highly affected by pore structure, strand size, and pore size (Freyman, Yannas, & Gibson, 2001; Kim & Son, 2009). Uniaxial tensile tests were performed to observe the effect of pore size on the mechanical properties of structured chitosan scaffolds. As shown in Fig. 6, both the tensile strength and modulus decreased as the pore size increased. The tensile properties of the scaffolds were closely related to porosity. For scaffolds with the same chitosan strand diameter, an increase in porosity (from 81% of C-100 to 90% of C-400) caused a decrease in the tensile modulus, from 1.2 MPa to 0.8 MPa, and strength, from 0.16 MPa to 0.07 MPa. These were both relatively low, compared with the same properties of trabecular bone (38–130 MPa). Thus, the scaffolds fabricated were not strong enough to support bone regeneration and would only be suitable for soft tissues. However, the mechanical properties might be improved by incorporating various composite systems containing synthetic polymers and/or ceramics, such as hydroxyapatite (Ang et al., 2002). Future studies will focus on strengthening the structured chitosan scaffolds with various cross-linking conditions and supplementary materials.

Fig. 7(a) shows cell proliferation results from MTT assays after 1, 3, and 7 days. The optical density (OD) was measured at 570 nm to evaluate the number of viable cells. A 3D spongy chitosan scaffold (Fig. 2(a)) was used as a control. Cell proliferation was evaluated on three different structured chitosan scaffolds (C-100, C-200, C-400) and the spongy scaffold. The OD of the structured scaffolds

(C-100, C-200, C-400) was lower than that of the spongy scaffold after 1 day. This is due to a low degree of initial attachment onto the structured scaffolds. The injected cells passed readily through the uniformly distributed pores, rather than attach to the chitosan strands. However, with increasing culture time, the degree of cell migration and the rate of cell proliferation on the structured scaffolds surpassed those of the spongy chitosan. Fig. 7(b) shows the cell growth rate for various scaffolds (spongy-type of chitosan, C-100, C-200, C-400). The growth rate was defined as an OD value of MTT assay/day and to calculate the value, the data were linearly fitted with commercial software (Origin 7.0). As shown in the data, the cryogenically designed scaffolds show higher cell growth rate than that of the spongy scaffold. In particular, the C-200 scaffold exhibited the highest cell proliferation rate. This was likely due to the more appropriate channels for cell migration. However, this result was confined to our structured scaffolds with microsized chitosan strands. The large pore size of the C-400 scaffold proved to be a significant obstacle to cell proliferation, while the small pore size of the C-100 scaffold inhibited cell migration. According to Murphy, Haugh, and O'Brien (2010), the effects of pore size are well known. Large pore sizes can reduce the surface area of the scaffold to a level that limits cell adhesion, and the cells simply migrate through the scaffold, or the level of cell-to-cell contact will be too low to allow for proliferation and subsequent osteogenesis (Murphy et al., 2010).

Fig. 8(a)–(c) shows the cell morphologies for the spongy chitosan scaffold and C-200 structured scaffold. Fig. 8(a) shows that the cells had well spread over the surface of the spongy scaffold. However, the cross-sectional view shows that the spongy scaffold did not allow cells to grow in its interior, due to a lack of interconnected pores (Fig. 8(b)). In contrast, the scaffold in Fig. 8(c) shows good cell compactness around the pore throughout the uniformly distributed pore structure and enough coverage of the chitosan strands. These results contrast sharply with those observed with the spongy-type scaffold, in which cells grew primarily on the surface, and indicate that the chitosan scaffolds described here, with their highly porous and interconnected pore structures, can be useful as a matrix to enhance infiltration and proliferation of applied cells. Furthermore, the fabrication technique for these scaffolds was rapid and stable and may be useful in the regeneration of various tissues.

4. Conclusions

Highly porous and interconnected chitosan scaffolds were fabricated using a 3D plotting method, coupled with a cryogenic system. The method allows one to create design-based and surface-modified chitosan scaffolds. The scaffold pore size was readily controlled by tailoring process parameters and the chitosan scaffold remained extremely porous, even after cross-linking (>85%). Shrinkage and swelling of the final scaffold were within ±10% of the designed dimensions. Mechanical properties were highly dependent on the pore structure, which could be adjusted without changing the chitosan concentration. Cell proliferation on the structured scaffolds was higher than on conventional spongy-type scaffolds. In particular, scaffolds with 200-μm pores exhibited the highest rate of cell proliferation.

References

Ahn, S. H., Koh, Y. H., & Kim, G. H. (2010). A three-dimensional hierarchical collagen scaffold fabricated by a combined solid freeform fabrication (SFF) and electrospinning process to enhance mesenchymal stem cell (MSC) proliferation. *Journal of Micromechanics and Microengineering*, *20*, 065015.

Ahn, S. H., Yoon, H., Kim, G. H., Kim, Y. Y., Lee, S. H., & Chun, W. (2009). Designed three-dimensional collagen scaffolds for skin tissue regeneration. *Tissue Engineering Part C: Methods*, doi:10.1089/ten (ahead of print)

Ang, T. H., Sultana, F. S. A., Hutmacher, D. W., Wong, Y. S., Fuh, J. Y. H., Mo, X. M., et al. (2002). Fabrication of 3D chitosan–hydroxyapatite scaffolds using a robotic dispensing system. *Materials Science and Engineering C*, *20*, 35–42.

Choi, S. W., Xie, J., & Xia, Y. (2009). Chitosan-based inverse opals: Three-dimensional scaffolds with uniform pore structures for cell culture. *Advanced Materials*, *21*, 2997–3001.

Dalby, M. J., Giannaras, D., Riehle, M. O., Gadegaar, N., Affrossman, S., & Curtis, A. S. G. (2004). Rapid fibroblast adhesion to 27 nm high polymer demixed nanotopography. *Biomaterials*, *25*, 77–83.

Dalton, P. D., Woodfield, T., & Hutmacher, D. W. (2009). Snapshot: Polymer scaffolds for tissue engineering. *Biomaterials*, *30*, 701–702.

Drury, J. L., & Mooney, D. J. (2003). Hydrogels for tissue engineering: Scaffold design variables and applications. *Biomaterials*, *24*, 4337–4351.

Freyman, T. M., Yannas, I. V., & Gibson, L. J. (2001). Cellular materials as porous scaffolds for tissue engineering. *Progress in Materials Science*, *46*, 273.

Gadegaard, N., Martines, E., Riehle, M. O., Seunarine, K., & Wilkinson, C. D. W. (2006). Applications of nano-patterning to tissue engineering. *Microelectronic Engineering*, *83*, 1577–1581.

Glowacki, J., & Mizuno, S. (2008). Collagen scaffolds for tissue engineering. *Biopolymers*, *89*, 338–344.

Hollister, S. J. (2005). Porous scaffold design for tissue engineering. *Nature Materials*, *4*, 518–524.

Huang, Y., Siewe, M., & Madihally, S. V. (2006). Effect of spatial architecture on cellular colonization. *Biotechnology and Bioengineering*, *93*, 64–75.

Hutmacher, D. W. (2000). Scaffolds in tissue engineering bone and cartilage. *Biomaterials*, *21*, 2529–2543.

Hutmacher, D. W., Sittinger, M., & Risbud, M. V. (2004). Scaffold-based tissue engineering: Rationale for compute-aided design and solid free-form fabrication systems. *Trends in Biotechnology*, *22*, 354–362.

Jamal, M., Bassik, N., Cho, J.-H., Randall, C. L., & Gracias, D. H. (2010). Directed growth of fibroblasts into three dimensional micropatterned geometries via self-assembling scaffolds. *Biomaterials*, *31*, 1683–1690.

Jiankang, H., Dichen, L., Yaxiong, L., Bo, Y., Hanxiang, Z., Qin, L., et al. (2009). Preparation of chitosan–gelatin hybrid scaffolds with well-organized microstructures for hepatic tissue engineering. *Acta Biomaterialia*, *5*, 453–461.

Karagenorgiou, V., & Kaplan, D. (2005). Porosity of 3D biomaterial scaffold and osteogenesis. *Biomaterials*, *26*, 5474–5491.

Kim, G. H., Ahn, S. H., Yoon, H., Kim, Y. Y., & Chun, W. (2009). A cryogenic direct-plotting system for fabrication of 3D collagen scaffolds for tissue engineering. *Journal of Materials Chemistry*, *19*, 8817–8823.

Kim, G. H., & Son, J. G. (2009). 3D polycaprolactone (PCL) scaffold with hierarchical structure fabricated by a piezoelectric transducer (PZT)-assisted bioplotter. *Applied Physics A*, *94*, 781–785.

Kim, I.-Y., Seo, S.-J., Moon, H.-S., Yoo, M.-K., Park, I.-Y., Kim, B.-C., et al. (2008). Chitosan and its derivatives for tissue engineering applications. *Biotechnology Advances*, *26*, 1–21.

Kim, S. J., Jang, D. H., Park, W. H., & Min, B.-M. (2010). Fabrication and characterization of 3-dimensional PLGA nanofiber/microfiber composite scaffolds. *Polymer*, *51*, 1320–1327.

Lawrence, B. J., & Madihally, S. V. (2008). Cell colonization in degradable 3D porous matrices. *Cell Adhesion & Migration*, *2*, 9–16.

Liao, C. J., Chen, C. F., Chen, J. H., Chiang, S. F., Lin, Y. J., & Chang, K. Y. (2002). Fabrication of porous biodegradable polymer scaffolds using a solvent merging/particulate leaching method. *Journal of Biomedical Materials Research*, *59*, 676–681.

Ma, P. X., & Choi, J. (2001). Biodegradable polymer scaffolds with well-defined interconnected spherical pore network. *Tissue Engineering*, *7*, 23–33.

Matthews, J. A., Wnek, G. E., Simpson, D. G., & Bowlin, G. L. (2002). Electrospinning of collagen nanofibers. *Biomacromolecules*, *3*, 232–238.

Mooney, D. J., Baldwin, D. F., Suh, N. P., Vacanti, J. P., & Langer, R. (1996). Novel approach to fabricate porous sponges of poly(D,L-lactic-co-glycolic acid) without the use of organic solvents. *Biomaterials*, *17*, 1417–1422.

Moroni, L., Schotel, R., Hammann, D., de Wijn, J. R., & van Blitterswijk, C. A. (2008). 3D fiber-deposited electrospun integrated scaffolds enhance cartilage tissue formation. *Advanced Functional Materials*, *18*, 53–60.

Murphy, C. M., Haugh, M. G., & O'Brien, F. J. (2010). The effect of mean pore size on cell attachment, proliferation and migration in collagen–glycosaminoglycan scaffolds for bone tissue engineering. *Biomaterials*, *31*, 461–466.

Oh, S. H., Park, I. K., Kim, J. M., & Lee, J. H. (2007). In vitro and in vivo characteristics of PCL scaffolds with pore size gradient fabricated by a centrifugation method. *Biomaterials*, *28*, 1664–1671.

Vieira, R. S., & Beppu, M. M. (2006). Interaction of natural and crosslinked chitosan membranes with Hg(II) ions. *Colloids and Surfaces A: Physicochemical and Engineering Aspects*, *279*, 196–207.

Williams, J. L., & Lewis, J. L. (1982). Properties and an anisotropic model of cancellous bone from the proximal tibial epiphysis. *Journal of Biomechanical Engineering*, *104*, 50–56.

Yang, S., Leong, K., Du, Z., & Chua, C.-K. (2001). Design of scaffolds for use in tissue engineering. Part I. Traditional factors. *Tissue Engineering*, *7*, 679–689.

Yoon, H., Ahn, S. H., & Kim, G. H. (2009). Three-dimensional polycaprolactone hierarchical scaffolds supplemented with natural biomaterials to enhance mesenchymal stem cell proliferation. *Macromolecular Rapid Communication*, *30*, 1632–1637.

Yoon, J. J., & Park, T. G. (2001). Degradation behaviors of biodegradable macroporous scaffolds prepared by gas foaming of effervescent salts. *Journal of Biomedical Materials Research*, *55*, 401–408.